Journal of Volcanology and Geothermal Research 393 (2020) 106806

Contents lists available at ScienceDirect

Journal of Volcanology and Geothermal Research

journal homepage: www.elsevier.com/locate/jvolgeores

The interaction between active crustal faults and volcanism: A case study of the Liquiñe-Ofqui Fault Zone and Osorno volcano, Southern Andes, using magnetotellurics

Daniel Díaz [a,b,*], Felipe Zúñiga [a], Angelo Castruccio [b,c]

[a] Departamento de Geofísica, Universidad de Chile, Blanco Encalada 2002, Santiago, Chile
[b] Centro de Excelencia en Geotermia de Los Andes, Plaza Ercilla 803, Santiago, Chile
[c] Departamento de Geología, Universidad de Chile, Plaza Ercilla 803, Santiago, Chile

ARTICLE INFO

Article history:
Received 9 August 2019
Received in revised form 24 January 2020
Accepted 30 January 2020
Available online 8 February 2020

Keywords:
Magnetotellurics
Electrical resistivity
Southern Andes
Magma reservoir

ABSTRACT

The relationship between subduction in convergent margins, crustal structures and magmatism is crucial to understand processes such as the type and frequency of volcanic activity in these areas. Although it is well known that the release of fluids by the subducting slab is the main cause of the arc volcanism in areas like the Central and Southern Andes, details such as the timing and pathways of magma ascent and storage are still not well understood. A key factor that needs to be better studied in the Southern Volcanic Zone of the Andes of Chile is the role of large tectonic features in fluid transport and magma ascent processes, such as the Liquiñe-Ofqui Fault Zone, a N-S strike-slip crustal structure parallel to the main volcanic arc. In this study, we focus on Osorno volcano, a stratovolcano composed mainly by products of basaltic to basaltic-andesite composition with minor dacites and with historical Hawaiian-Strombolian eruptions. Through the measurement of magnetotellurics and the use of 3-D modeling tools and petrologic constraints, two magmatic reservoirs have been inferred, which suggest a complex magmatic system with reservoirs of different depths and compositions. The shallowest magmatic reservoir (4–8 km) has a dacitic composition, while the deepest one (7–15 km), has an andesitic composition instead. The shallow reservoir is located 2 km to the E of the volcano and the deepest one is located 10 km to the E. Considering that the Liquiñe-Ofqui Fault Zone is located 20 km to the E of the volcano, we suggest that eruptions of Osorno volcano are associated with the ascent of deep crustal basaltic magma enhanced by this master fault, reactivating the inferred reservoirs and the volcano.

1. Introduction

The configuration of the convergent margin of the Andes varies significantly along its more than 8000 km length, and also temporally. According to Haschke et al. (2006) the volcanic arc in Southern Chile (41°–46°S) shows stationary arc magmatism from 200 to 50 Ma, followed by trench retreat and arc widening from 50 to 28 Ma; arc narrowing from 28 to 8 Ma; and magmatic quiescence from 8 to 3 Ma, while volcanism from the Pliocene to the present has been concentrated in a narrow volcanic arc with magmatism focused along the Liquiñe-Ofqui fault zone (LOFZ), as can be observed in Fig. 1.

The Southern volcanic zone (SVZ) of the Andes, extending from 33° to 46°S, includes at least 60 historically and potentially active volcanic edifices in Chile and Argentina, three giant silicic caldera systems and numerous minor eruptive centers (Siebert and Simkin, 2002; Stern, 2004; Stern et al., 2007). The arc edifices range in size from cinder cones of few hundredths of m diameter to stratovolcanoes that rise 2000 m from their base and cover some hundred square kilometers (Völker et al., 2011). During recent years three volcanic eruptions of Sub-Plinian to Plinian type have occurred in this volcanic zone, in Chaitén (2008–2009), Cordón Caulle (2011) and Calbuco (2015) volcanoes, and 2 Hawaiian-Strombolian eruptions (Llaima 2008–2009 and Villarrica 2015).

The differences in eruptive style and products observed in the various parts of the SVZ are related to different magma compositions, volatile content and control of the LOFZ and other local fault systems in the ascent and emplacement of magmas. Our main objective is the geophysical characterization of the subsurface structure of Osorno volcano, a historically active volcano close to populated areas in the lakes district of Chile. The Osorno-Puntiagudo chain (OP), formed by volcanoes Osorno, La Picada, Puntiagudo and Cordón Cenizos, shows a postglacial eruptive evolution characterized by flank eruptions, with the generation of pyroclastic cones of basaltic composition and dacitic domes, while summit eruptions are associated with a more explosive character.

* Corresponding author at: Departamento de Geofísica, Universidad de Chile, Blanco Encalada 2002, Santiago, Chile.
E-mail address: ddiaz@dgf.uchile.cl (D. Díaz).

https://doi.org/10.1016/j.jvolgeores.2020.106806

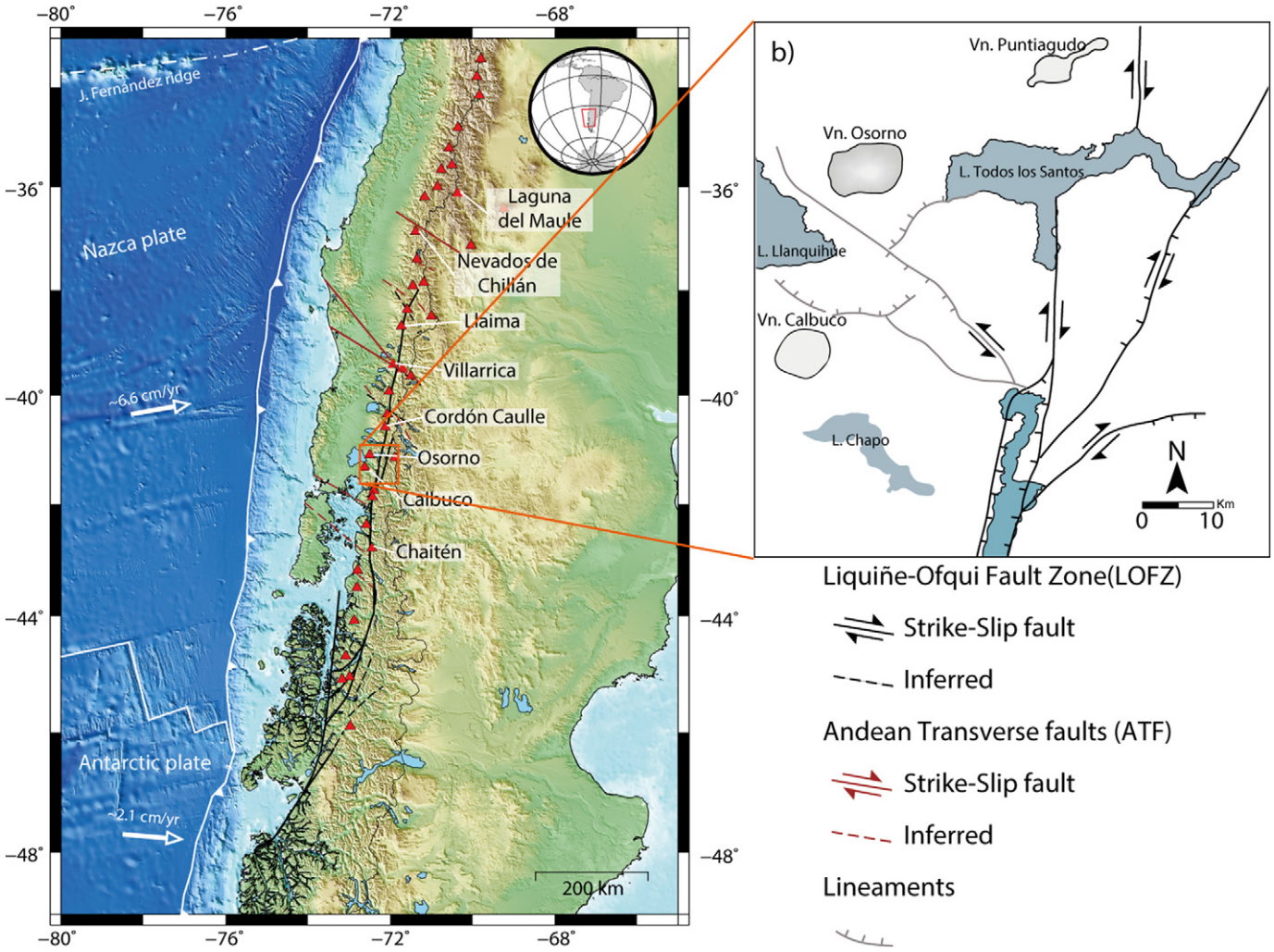

Fig. 1. Study area, showing in the left side the volcanoes of the Southern Volcanic zone of the Andes with Holocene activity (red triangles) and large scale tectonic features. Right side shows a zoomed view of the Liquiñe-Ofqui fault system around the Osorno volcano.

The last major eruptive activity of Osorno volcano was a fissure eruption in 1835, followed by only minor fumarolic activity during the 20th century. According to Moreno et al. (1979; 2010) the products of this volcanic chain are mainly basalts, while Calbuco volcano (40 km to the southwest) produce mainly andesites (Sellés and Moreno, 2011). López-Escobar et al. (1992) argued that the presence of amphibole-bearing andesites in Calbuco volcano can be due to a deeper crystallization zone and/or a significantly larger water content in the Calbuco magmatic system compared to Osorno.

In this subduction context, at shallow depths crustal fluids may circulate through a brittle crust which has been folded and fractured by tectonic deformation, while fluids released from the subducting slab enhance partial melting at lower crustal to upper mantle depths, by reducing the melting point of the rocks (Grove et al., 2012), proving a feeding zone for magmatic structures placed at shallower depths. These processes result in a considerable electrical conductivity enhancement at different levels in the crust, forming ideal targets to be identified by geophysical methods sensitive to this parameter, such as magnetotellurics.

2. Magnetotelluric data and analysis

Magnetotellurics (MT) is an electromagnetic sounding method which belongs to the geophysical techniques governed by the diffusion equation. Measurements of period-dependent fluctuations in the electric and magnetic fields on the surface of the Earth can be used to obtain information of the resistivity distribution in depth. As the resistivity of rocks in the Earth extends over a very wide range, the MT method is a useful tool to image the resistivity distribution of the subsurface, in shallow crustal to mantle depth studies. Several magnetotelluric studies have been developed in different volcanic zones around the world during the last years, interpreting electrical conductors as hydrothermal fluids (Manzella et al., 2004; Ingham et al., 2009; Bertrand et al., 2012), clays (Matsushima et al., 2001) and magmatic conduits or reservoirs (Hill et al., 2015; Aizawa et al., 2014; Díaz et al., 2015). This method is, therefore, widely used for the exploration of geothermal resources, as shown by Muñoz (2014).

In this work, magnetotelluric data has been measured in 16 sites around Osorno volcano, obtaining time series of 2 electric and 3 magnetic field components, as described in Fig. 2, using Metronix equipment. Good data quality of the measured data has been obtained due to measuring times of 24–48 h per site in a low cultural noise ambient, but the lack of accessibility routes made very difficult the measurement of more stations, particularly to the west of the volcano. Time series of the horizontal components of electric (E) and magnetic (H) fields, as well as the vertical component of the magnetic field (Hz) recorded at each measured station were processed using a robust processing code based on Egbert and Booker (1986), and Egbert (1997). From this robust processing, the complex impedance tensor (Z), defined as $E = ZH$ and geomagnetic transfer function (K), defined as $Hz = KH$ (Wiese, 1962) are estimated. Apparent resistivity and phase curves can be obtained

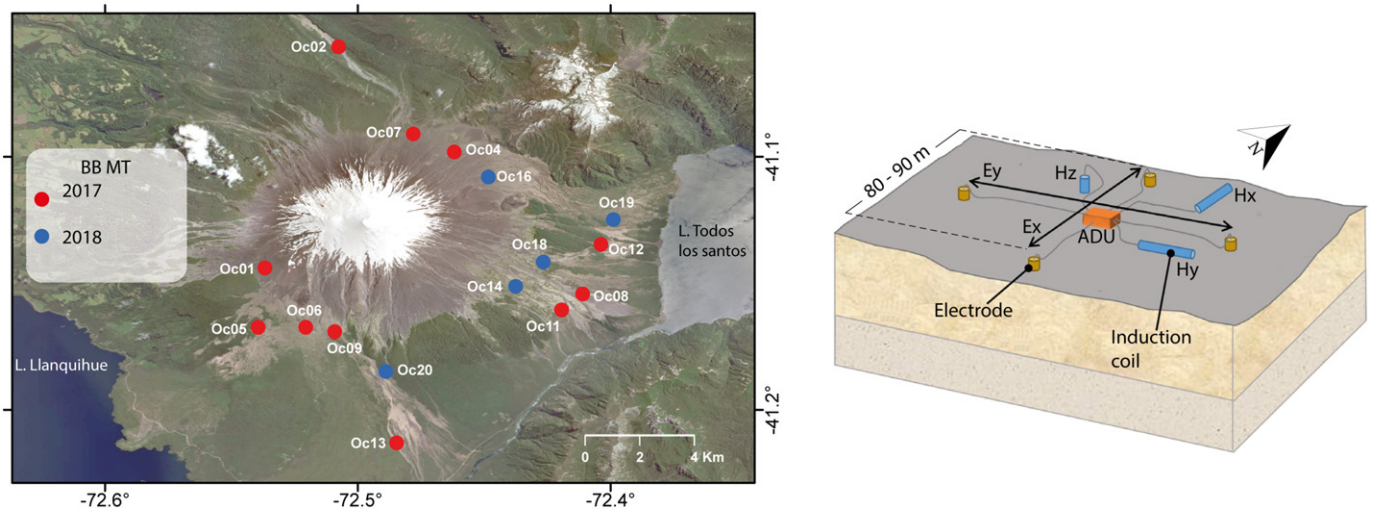

Fig. 2. Sites measured during 2017 and 2018 (left) and scheme of a broad-band measuring site (right).

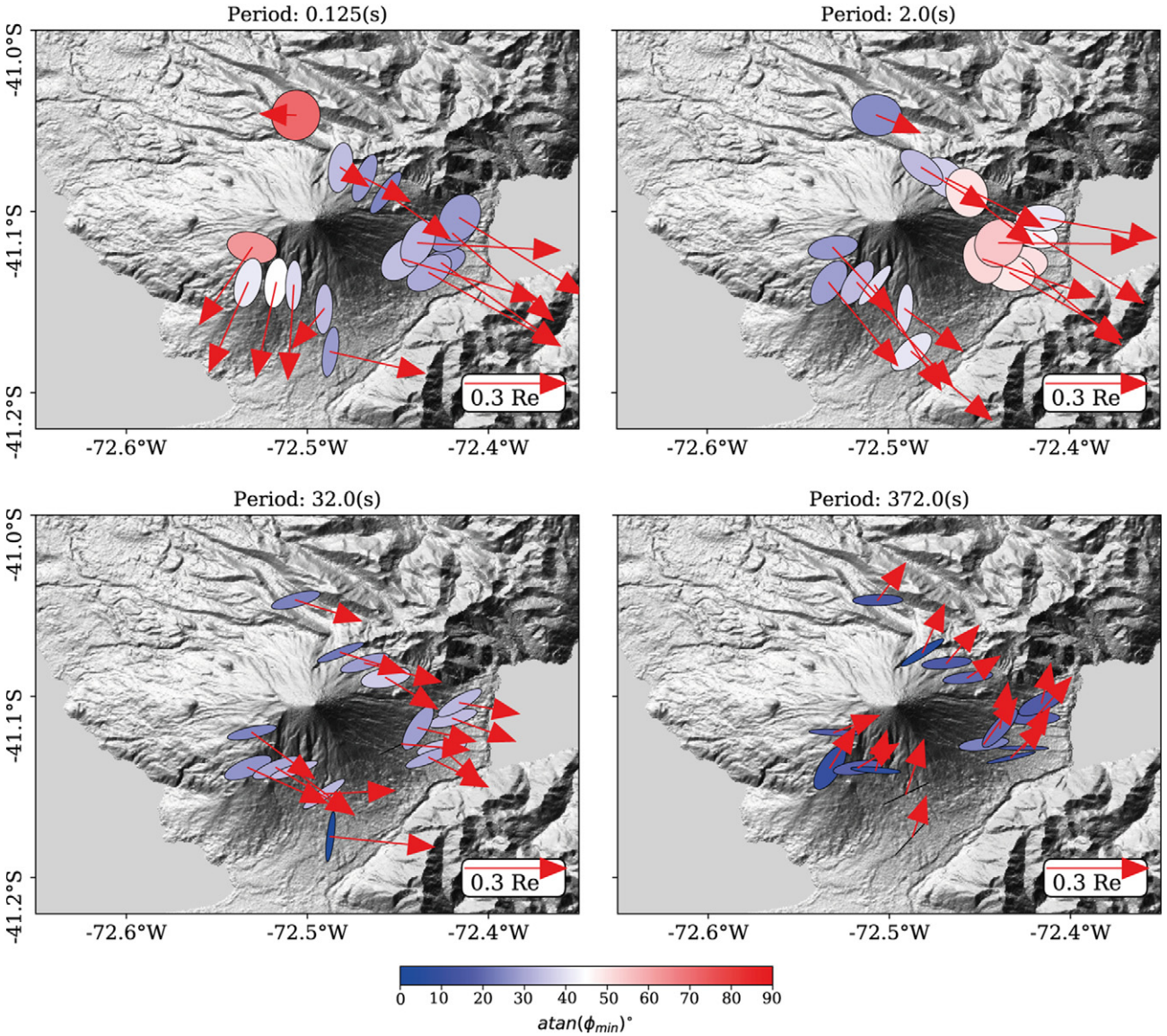

Fig. 3. Phase tensor ellipses and induction arrows (convention of Wiese) for periods of 0.125 s, 2 s, 32 s and 372 s.

from the calculated impedance tensors, as well as induction arrows from the geomagnetic transfer functions. In the presence of near surface heterogeneities, the amplitude of the observed electric field may be drastically distorted. The calculation of a phase tensor defined as $\Phi = \mathrm{Re}(Z)^{-1}\mathrm{Im}(Z)$, seeks then to recover the regional phase relationship from a set of distorted measurements, even when both the near surface heterogeneity and the regional conductivity structures are 3D (Caldwell et al., 2004). The phase tensor can be graphically represented by an ellipse with its principal axes (Φ_{max} and Φ_{min}). By plotting maps of phase tensor ellipses and induction vectors at different periods, main resistivity structures can be identified in the data before modeling, as can be observed in Fig. 3. As observed, the data shows large variability of electrical resistivity for short periods, but induction arrows and phase tensor ellipses start to identify larger scale structures at periods of 1–2 s, were a relatively conductive feature is observed at the eastern side of the volcano, but the induction arrows seem to be strongly influenced by a conductive feature to the W-NW. For periods larger than 32 s, the induction arrows seem to be very affected by a large-scale conductive feature to the W-SW, however this has been reported previously in the Southern Andes of Chile by Brasse et al. (2009), discarding the possible effect of the Pacific Ocean in the induction arrows behavior, and pointing to the influence of an electrical resistivity anisotropic zone in the crust to explain the strange behavior of the induction arrows. Note that the phase tensor ellipses for long periods (e.g. 372 s in Fig. 3) are not really affected by the NE trend of the anisotropy, but are related mainly to an E-W change in the resistivity distribution at depth.

3. Three dimensional modeling

3D inversion codes are a useful tool to generate models which can fit the measured data. Examples of such codes available for research are WSINV3DMT (Siripunvaraporn et al., 2005), and MODEM (Kelbert et al., 2014). We used MODEM to invert our dataset, which uses a finite differences approach and a nonlinear conjugate gradient scheme, considering the topography of the study area. As a starting model, a homogeneous resistivity of 500 Ohm-m was set, considering the presence of volcanic and metamorphic rocks in the upper crust of the study area, and also the presence of lakes of glacial origin as Todos Los Santos and Llanquihue. We measured the conductivity of these waters, obtaining values of the same magnitude (100–500 Ohm-m). Data in a period range between 0.00098 s–1024 s was considered, and error floors of 4% for the off-diagonal components and 8% for the diagonal ones. Considering the strong anisotropic effect observed in the induction arrows, the inversion of the geomagnetic transfer function was not considered. The full impedance tensor was inverted considering a grid of 82 × 64 × 121 cells in x, y and z respectively, considering the topography of the study area discretized from SRTM data. Minimum mesh size was 400 m × 400 m in x and y directions, in the central part of the mesh, while z increased from a minimum size of 300 m for the shallowest cells.

4. Resulting models and petrologic constraints

As shown in Fig. 4, and discussed in the previous section, two relatively low resistivity anomalies are observed at different depths, below and to the east of Osorno volcano. Several tests have been performed to check the reliability of these features, considering different initial model values and the substitution of C1 and/or C2 anomalies for 500 Ohm-m values, as shown in Fig. 5 and Supplementary material. The shape and location of the obtained anomalies remain when changing initial resistivity values and error floors tested (between 4% and 10% for different components). Different initial resistivity values have an influence in the resistivity of the obtained anomalies C1 and C2, but worst data fits were obtained compared to the selected model using 500 Ohm-m. From the selected model presented in Fig. 4, the shallowest anomaly extends between 4 and 8 km below sea level, reaching resistivities of 115–230 Ohm-m, and a second one which is deeper between 7 and 15 km below the sea level, and reaching resistivities between 40 and 115 Ohm-m. These resistivity values are not as low as one could expect in a volcanic environment, but still could represent magmatic reservoirs

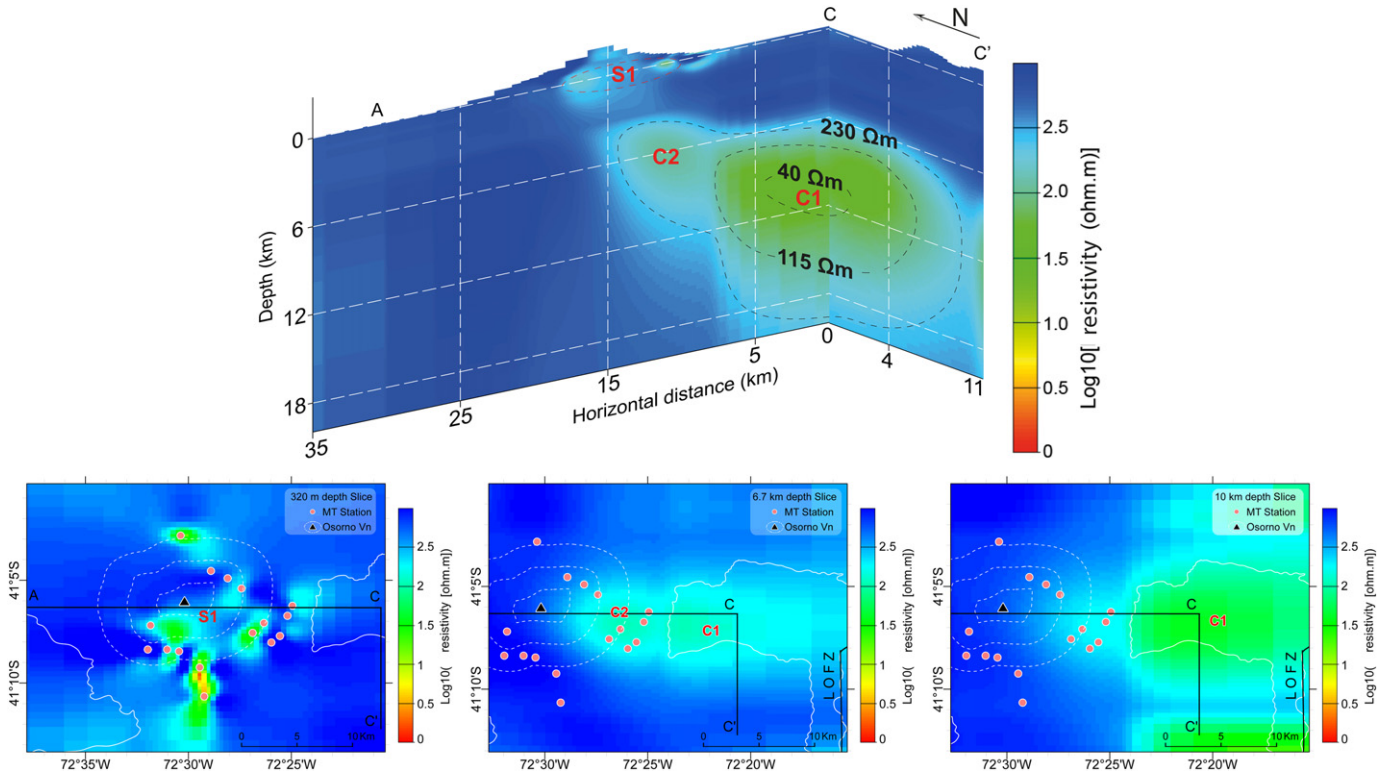

Fig. 4. Final model obtained from the 3-D inversion, shown as plan views (down) and vertical slices (up). Location of vertical slices is shown in the plan views.

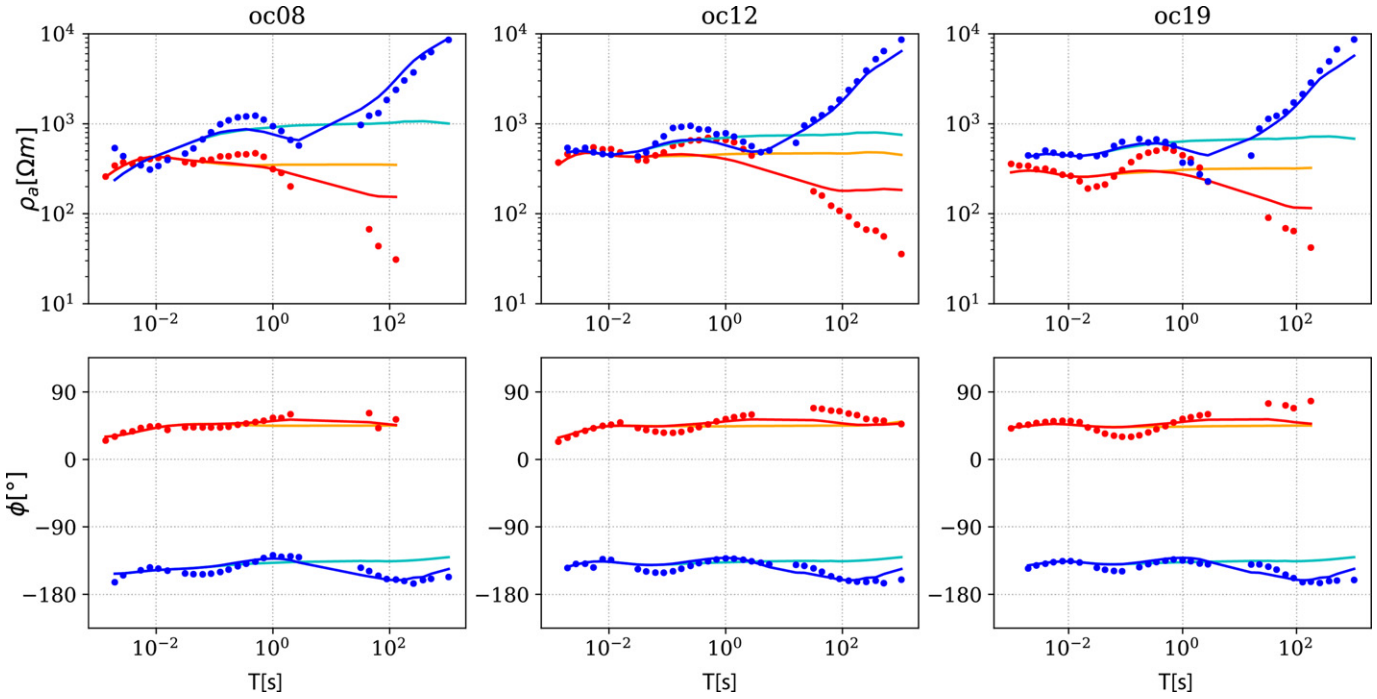

Fig. 5. Apparent resistivity and phase curves of the off-diagonal components, calculated from measured data (red dots Zxy component, blue dots Zyx component), best model shown in Fig. 4 (red lines Zxy component, blue lines Zyx component) and sensitivity test considering the replace of values smaller than 230 Ohm-m for C1 and smaller than 115 Ohm-m for C2, with a resistivity of 500 Ohm-m (orange line Zxy component, cyan line Zyx component).

if the expected magmatic composition and storage conditions are considered, in particular the high expected resistivity of the surrounding material.

According to López-Escobar et al. (1992), the youngest Osorno products are characterized by basaltic to basaltic andesites, however dacitic domes at the western and southern flank of the volcano have been identified (see Moreno et al., 2010). This suggest the existence of more than one magmatic reservoir related to Osorno volcano, and a possible differentiation with depth as interpreted with geophysical observations in other volcanic systems of the Central Andes (Pritchard et al., 2018).

In this case, various options of composition and storage conditions were tested, considering a ranged variability of diverse parameters such as SiO_2 magmatic content, temperature and pressure conditions, wt% H_2O and partially molten rate, with all these parameters changing significantly the resistivity of a magmatic reservoir. The variability of electrical resistivity with all the above mentioned parameters can be seen in Pommier and Le-Trong (2011), Laumonier et al. (2015) and Guo et al. (2017).

Based on the identification of two structures with different resistivity values (C1 and C2), and considering the variable volcanic products observed in Osorno volcano, a magmatic system considering two different reservoirs at different depths is presented, with different magma types and reservoir conditions. This kind of model has been already presented in other volcanic systems in the world, in particular for volcanoes with similar petrologic conditions as Osorno. For Fuji volcano (Japan), Miyaji et al. (2011) presented a schematic model of the magma plumbing system for a historic eruption, considering a shallow dacitic reservoir (5–10 km) and a deeper (10–15 km) andesitic reservoir, both affected by the influence of basaltic magma ascending from deeper dyke structures.

One general condition observed in the last eruptive processes of Osorno volcano is the low water content, ranging between 0.22 and 0.73 wt% H_2O in bulk rocks (Tagiri et al., 1993), while pre-eruptive values have been estimated between 1 and 2 wt% H_2O by Morgado et al. (2018). Considering this as a common feature for the whole magmatic system, different values of temperature, pressure and composition were selected for the 2 reservoirs. Considering C1 as a deeper andesitic magma reservoir, its temperature ranges between 1000 and 1100 °C and a pressure is defined for a depth of 10 km according to the corresponding lithostatic gradient based on Cas and Simmons (2018). On the other hand, C2 should be a shallower dacitic magma accumulation, with a temperature ranging between 820 and 920 °C and pressure corresponding to 6 km depth, based on the previously mentioned analysis. To estimate the electrical resistivity of these magmatic reservoirs, we decided to use melt-specific models presented by Guo et al. (2017), considering that according to these authors, SIGMELTS (Pommier and Le-Trong, 2011) significantly underestimates the influence of H_2O on electrical conductivity estimations, and this value is well constrained (particularly small) by geologic observations in Osorno volcano. Resistivity estimations calculated for these cases, considering variable water content are shown in Fig. 6.

Electrical resistivity estimations for these magmas result in 0.99 to 11.30 Ohm-m for the andesitic reservoir (C1) and 3.80 to 25 Ohm-m for the dacitic reservoir (C2). These values are much lower than the resistivity values obtained by the 3-D model, but assume a 100% melt rate in the reservoirs. More realistic melt rates were estimated for both cases using Hashin-Shtrikman upper bounds (Hashin and Shtrikman, 1963), considering a two-phase material with the estimated magma resistivity values for each reservoir, and a surrounding rock of 500 Ohm-m. Melt fraction estimations (shown in Fig. 6) range between 2 and 13% for the dacitic reservoir (C2) and 4–36% for the andesitic reservoir (C1), fitting the resistivity values obtained for both anomalies in the 3-D inversion process.

As most of the eruptive products from Osorno volcano are basalts, these results imply that the feeding source of magma during eruptions is located at deeper zones and interact little with the magma bodies identified in this work. Koulakov et al. (2013) showed using seismic tomography that at Klyuchevskoy volcano, Russia, there are several levels of temporal storage of magma at the upper and intermediate crust that are active only during eruptions and that these storage zones are fed by a permanent source located at the interface between the crust and mantle. At Osorno volcano, there could be a similar magmatic system, where

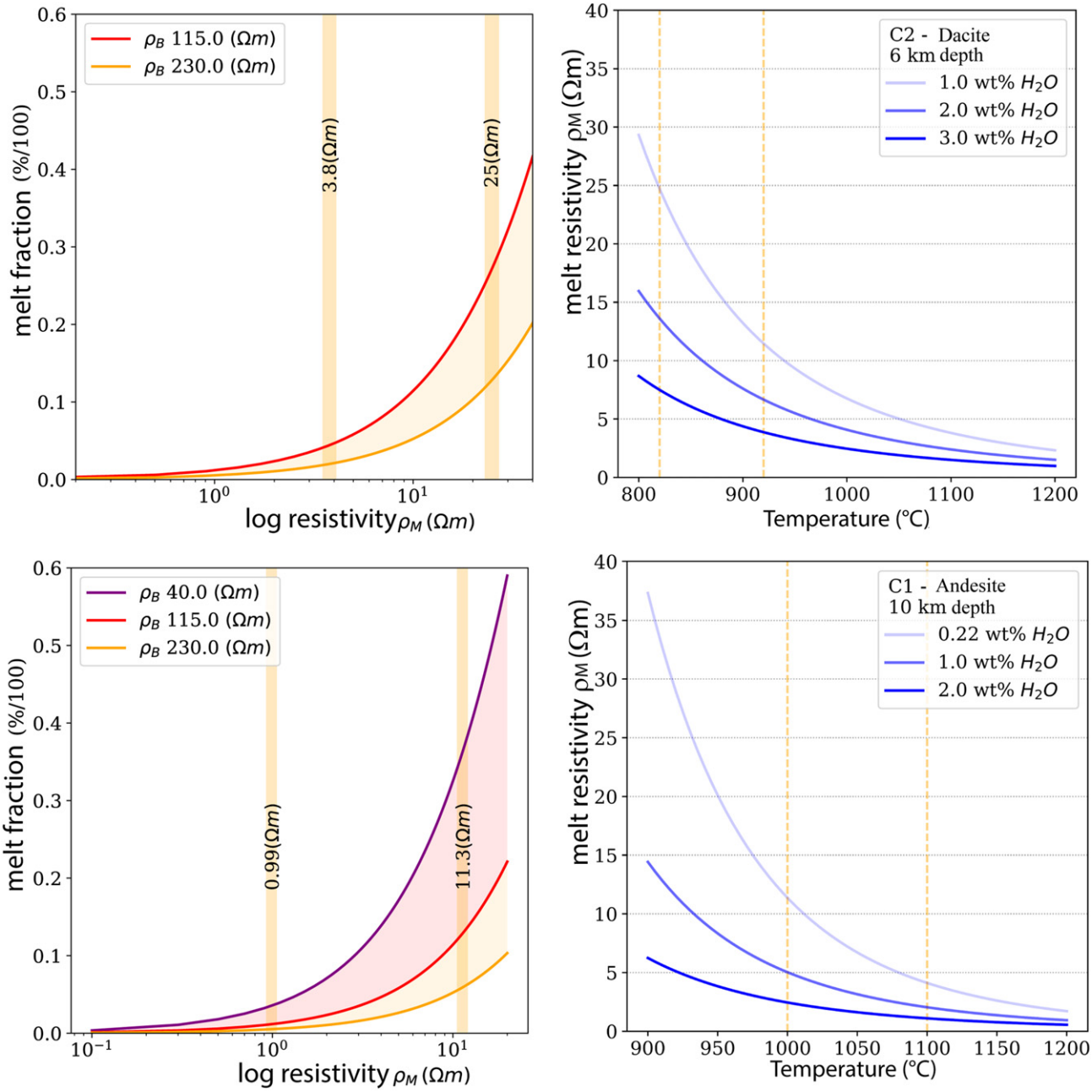

Fig. 6. Resistivities of melt (left) and bulk (right) for the deep (up) and shallow (down) reservoirs.

shallow basaltic magma chambers suggested by thermobarometry (Morgado et al., 2018) are not currently present, but are generated during eruptive activity. Morgado et al. (2018) also suggested the presence of a crystal mush-type reservoir with a maximum depth of 4.5 km that could be correlated with the shallow reservoir modelled in this study.

5. Conclusions

The 3-D modeling of magnetotelluric data measured around Osorno volcano points to the presence of two magmatic reservoirs extending to the east of the volcanic edifice. These conductive anomalies, considering the resistivity values obtained for the model with the best data fit, could be explained by dacitic and andesitic reservoirs with variable melt rates that seem strongly controlled by the presence of the large scale Liquiñe-Ofqui Fault Zone, crossing just below the Todos Los Santos lake in this area. Different modeling tests performed with this data set, show that size and location of C1 and C2 are reliable, even when resistivity values of these anomalies could vary. The influence of the referred large scale fault system is clear in the distribution of volcanoes in the Southern Andes of Chile, and its relation with second order NE and NW lineaments is associated with the small scale tectonic regime and the eruptive products of different volcanoes in the SVZ as shown by López-Escobar et al. (1995) and Cembrano and Lara (2009). Even when young NE volcanic lineaments of the SVZ, as Osorno-Puntiagudo, have been related to basaltic to basaltic-andesitic products and therefore short residence times of magmas in the crust, geophysical evidence worldwide point to the complexity of volcanic systems (e.g. Pritchard et al., 2018; Cordell et al., 2018; Hata et al., 2018) and the presence of a silica rich reservoir closer to the surface is supported by the presence of dacitic domes and cones in the flanks of Osorno and Holocene pumiceous fall deposits distributed to the east of this volcano. A possible plumbing system for Osorno volcano is shown in Fig. 7, where both dacitic and andesitic reservoirs lay close to the Liquiñe-Ofqui fault system that could enhance deep magma ascent as dykes, through a

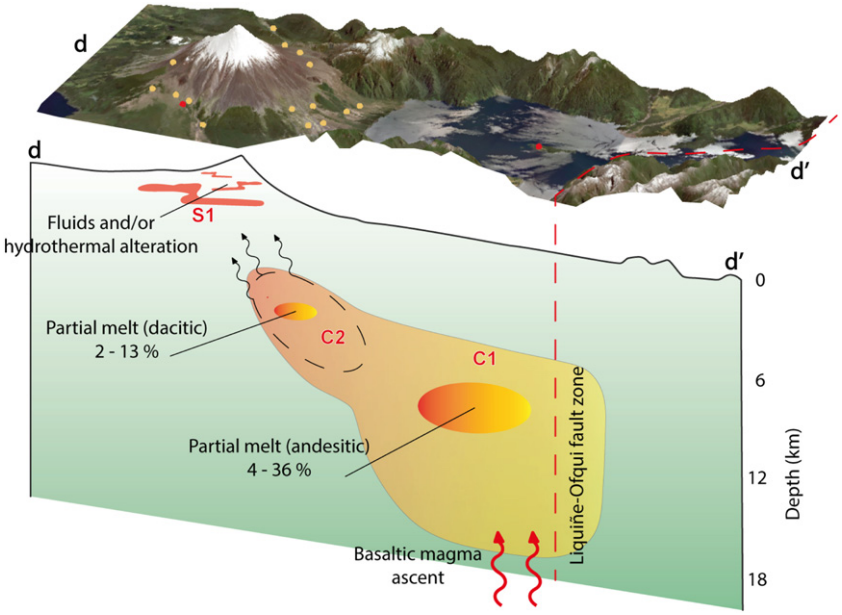

Fig. 7. Interpretative scheme considering final 3-D resistivity model and petrologic constrains.

composite system of tensional and shear fractures, in an overall strike-slip regime, but oriented subparallel to the maximum horizontal stress (Cembrano and Lara, 2009). These N-E oriented dyke swarms within the crust could be an explanation to the electrical resistivity anisotropy inferred in this work as well as in other works in south Chile (Soyer, 2002; Brasse et al., 2009), as suggested by Soyer (2002).

Supplementary data to this article can be found online at https://doi.org/10.1016/j.jvolgeores.2020.106806.

Abbreviations

MT	magnetotellurics
LOFZ	Liquiñe-Ofqui Fault Zone
SVZ	Southern Volcanic Zone of the Andes
O-P	Osorno Puntiagudo chain

CRediT authorship contribution statement

Daniel Díaz: Conceptualization, Methodology, Software, Investigation, Validation, Writing - original draft, Writing - review & editing, Project administration, Funding acquisition. **Felipe Zuñiga:** Investigation, Formal analysis, Validation, Visualization. **Angelo Castruccio:** Investigation, Writing - review & editing.

Declaration of competing interest

The authors declare that they have no known competing financial interests or personal relationships that could have appeared to influence the work reported in this paper.

Acknowledgements

We would like to thank CONAF (Corporación Nacional Forestal, Chile) for providing access to the surroundings of Osorno volcano, part of the Vicente Pérez Rosales National Park. Thanks to Eric Cárdenas, Karin García, Romina Gutierrez, María José Hernández, Daniela Montecinos, Luna Pérez, Felipe Reyes, Nicolás Vera and Vicente Yáñez for their support in field work activities. This work was funded by FONDECYT 1170195. We thank the support from PIA/CONICYT Anillo ACT-172002 and Centro de Excelencia en Geotermia de Los Andes (FONDAP 15090013). Lastly, we thank two reviewers for their useful comments, which greatly improved the manuscript.

References

Aizawa, K., Koyama, T., Hase, H., Uyeshima, M., Kanda, W., Utsugi, M., Yoshimura, R., Yamaya, Y., Hashimoto, T., Yamazaki, K., Komatsu, S., Watanabe, A., Miyakawa, K., Ogawa, Y., 2014. Three-dimensional resistivity structure and magma plumbing system of the Kirishima Volcanoes as inferred from broadband magnetotelluric data. J. Geophys. Res. Solid Earth 119, 198–215. https://doi.org/10.1002/2013JB010682.

Bertrand, E.A., Caldwell, T.G., Hil, G.J., Wallin, E.L., Bennie, S.L., Cozens, N., Onacha, S.A., Ryan, G.A., Walter, C., Zaino, A., Wameyo, P., 2012. Magnetotelluric imaging of upper-crustal convection plumes beneath the Taupo Volcanic Zone, New Zealand. Geophys. Res. Lett. 39, L02304. https://doi.org/10.1029/2011GL050177.

Brasse, H., Kapinos, G., Li, Y., Mütschard, L., Soyer, W., Eydam, D., 2009. Structural electrical anisotropy in the crust at the South-Central Chilean continental margin as inferred from geomagnetic transfer functions. Phys. Earth Planet. Inter. 173, 7–16. https://doi.org/10.1016/j.pepi.2008.10.017.

Caldwell, T.G., Bibby, H.M., Brown, C., 2004. The magnetotelluric phase tensor. Geophys. J. Int. 158, 457–469.

Cas, R.A., Simmons, J.M., 2018. Why deep-water eruptions are so different from subaerial eruptions. Front. Earth Sci. 6, 198. https://doi.org/10.3389/feart.2018.00198.

Cembrano, J., Lara, L., 2009. The link between volcanism and tectonics in the southern volcanic zone of the Chilean Andes: a review. Tectonophysics 471, 96–113. https://doi.org/10.1016/j.tecto.2009.02.038.

Cordell, D., Unsworth, M., Díaz, D., 2018. Imaging the Laguna del Maule Volcanic Field, central Chile using magnetotellurics: evidence for crustal melt regions laterally-offset from surface vents and lava flows. Earth Planet. Sci. Lett. 488, 168–180. https://doi.org/10.1016/j.epsl.2018.01.007.

Díaz, D., Heise, W., Zamudio, F., 2015. Three-dimensional resistivity image of the magmatic system beneath Lastarria volcano and evidence for magmatic intrusion in the back arc (northern Chile). Geophys. Res. Lett. 42. https://doi.org/10.1002/2015GL064426.

Egbert, G., 1997. Robust multiple-station magnetotelluric data processing. Geophys. J. Int. 130, 475–496.

Egbert, G., Booker, J.R., 1986. Robust estimation of geomagnetic transfer functions. Geophys. J. R. Astron. Soc. 87, 173–194.

Grove, T.L., Till, C.B., Krawczynski, M.J., 2012. The role of H2O in subduction zone magmatism. Annu. Rev. Earth Planet. Sci. 40, 413–439.

Guo, X., Li, B., Ni, H., Mao, Z., 2017. Electrical conductivity of hydrous andesitic melts pertinent to subduction zones. J. Geophys. Res. Solid Earth 122 (3), 1777–1788.

Haschke, M., Günther, A., Melnick, D., Echtler, H., Reutter, K.J., Scheuber, E., Oncken, O., 2006. Central and southern Andean tectonic evolution inferred from arc magmatism. In: Oncken, et al. (Eds.), The Andes: Active Subduction Orogeny, Frontiers in Earth Sciences. Springer-Verlag, pp. 337–353 (Berlin, Germany).

Hashin, Z., Shtrikman, S., 1963. A variational approach to the theory of the elastic behaviour of multiphase materials. J. Mech. Phys. Solids 11 (2), 127–140.

Hata, M., Matsushima, N., Takakura, S., Utsugi, M., Hashimoto, T., Uyeshima, M., 2018. Three-dimensional electrical resistivity modeling to elucidate the crustal magma supply system beneath Aso caldera, Japan. J. Geophys. Res. Solid Earth 123, 6334–6346. https://doi.org/10.1029/2018JB015951.

Hill, G.J., Bibby, H.M., Ogawa, Y., Wallin, E.L., Bennie, S.L., Caldwell, T.G., Keys, H., Bertrand, E.A., Heise, W., 2015. Structure of the Tongariro Volcanic system: insights from magnetotelluric imaging. Earth Planet. Sci. Lett. 432, 115–125. https://doi.org/10.1016/j.epsl.2015.10.003.

Ingham, M.R., Bibby, H.M., Heise, W., Jones, K.A., Cairns, P., Dravitzki, S., Bennie, S.L., Caldwell, T.G., Ogawa, Y., 2009. A magnetotelluric study of Mount Ruapehu volcano, New Zealand. Geophys. J. Int. 179, 887–904.

Kelbert, A., Meqbel, N., Egbert, G.D., Tandon, K., 2014. ModEM: a modular system for inversión of electromagnetic geophysical data. Comput. Geosci. 66, 40–53. https://doi.org/10.1016/j.cageo.2014.01.010.

Koulakov, I., Gordeev, E.I., Dobretsov, N.L., Vernikovsky, V.A., Senyukov, S., Jakovlev, A., Jaxybulatov, K., 2013. Rapid changes in magma storage beneath the Klyuchevskoy group of volcanoes inferred from time-dependent seismic tomography. J. Volcanol. Geotherm. Res. 263, 75–91.

Laumonier, M., Gaillard, F., Sifré, D., 2015. The effect of pressure and water concentration on the electrical conductivity of dacitic melts: implication for magnetotelluric imaging in subduction areas. Chem. Geol. 418, 66–76.

López-Escobar, L., Parada, M.A., Moreno, H., Frey, F., Hickey-Vargas, R.L., 1992. A contribution to the petrogenesis of Osorno and Calbuco volcanoes, Southern Andes (41°00′-41°30′S): comparative study. Rev. Geol. Chile 19 (2), 211–226.

López-Escobar, L., Cembrano, J., Moreno, H., 1995. Geochemistry and tectonics of the Chilean Southern Andes basaltic Quaternary volcanism (37-46 S). Andean Geol. 22 (2), 219–234.

Manzella, A., Volpi, G., Zaja, A., Meju, M., 2004. Combined TEM-MT investigation of shallow-depth resistivity structure of Mt. Somma-Vesuvius. J. Volcanol. Geotherm. Res. 131, 19–32.

Matsushima, N., Oshima, O., Ogawa, Y., Takakura, S., Satoh, H., Utsugi, M., Nishida, Y., 2001. Magma prospecting in Usu volcan, Hokkaido, Japan, using magnetotelluric soundings. J. Volcanol. Geotherm. Res. 109, 263–277.

Miyaji, N., Kan'no, A., Kanamaru, T., Mannen, K., 2011. High-resolution reconstruction of the Hoei eruption (AD 1707) of Fuji volcano, Japan. J. Volcanol. Geotherm. Res. 207 (3–4), 113–129.

Moreno, H., Naranjo, J.A., López, L., 1979. Geología y petrología de la cadena volcánica Osorno-Puntiagudo, Andes del Sur, latitud 41°10′S. Segundo Congreso Geológico Chileno, Arica, Chile.

Moreno, H., Lara, L., Orozco, G., 2010. Geología del volcán Osorno: Región de Los Lagos. Servicio Nacional de Geología y Minería, Chile.

Morgado, E., Morgan, D.J., Harvey, J., Parada, M.A., Castruccio, A., Brahm, R., 2018. Erupción de 1835 del Volcán Osorno: condiciones intensivas y escalas de tiempo calculadas a través de difusión de múltiples elementos en olivino. Abstracts of the XV Congreso Geológico Chileno. Universidad de Concepción, Chile (18–23 November 2018).

Muñoz, G., 2014. Exploring for geothermal resources with electromagnetic methods. Surv. Geophys. 35, 101–122. https://doi.org/10.1007/s10712-013-9236-0.

Pommier, A., Le-Trong, E., 2011. "SIGMELTS": a web portal for electrical conductivity calculations in geosciences. Comput. Geosci. 37 (9), 1450–1459.

Pritchard, M.E., de Silva, S.L., Michelfelder, G., Zandt, G., McNutt, S.R., Gottsmann, J., West, M.E., Blundy, J., Christensen, D.H., Finnegan, N.J., Minaya, E., Sparks, R.S.J., Sunagua, M., Unsworth, M.J., Alvizuri, C., Comeau, M.J., del Potro, R., Díaz, D., Diez, M., Farrell, A., Henderson, S.T., Jay, J.A., Lopez, T., Legrand, D., Naranjo, J.A., McFarlin, H., Muir, D., Perkins, J.P., Spica, Z., Wilder, A., Ward, K.M., 2018. Synthesis: PLUTONS: investigating the relationship between pluton growth and volcanism in the Central Andes. Geosphere 14 (3), 1–29. https://doi.org/10.1130/GES01578.1.

Sellés, D., Moreno, H., 2011. Geología del volcán Calbuco, Región de los Lagos. Servicio Nacional de Geología y Minería. Carta Geológica de Chile, Serie Geología Básica 20 (1).

Siebert, L., Simkin, T., 2002. Volcanoes of the World: An Illustrated Catalog of Holocene Volcanoes and Their Eruptions. Smithsonian Institution Global Volcanism Program Digital Information Series.

Siripunvaraporn, W., Egbert, G., Lenbury, Y., Uyeshima, M., 2005. Three-dimensional magnetotelluric inversion: data-space method. Phys. Earth Planet. Inter. 50, 3–14.

Soyer, W., 2002. Analysis of Geomagnetic Variations in the Central and Southern Andes. Ph.D. Thesis. Freie Univerität, Berlin (135 pp.).

Stern, C.R., 2004. Active Andean volcanism: its geologic and tectonic setting. Rev. Geol. Chile 31 (2), 161–206.

Stern, C.R., Moreno, H., López-Escobar, L., Clavero, J.E., Lara, L.E., Naranjo, J.A., Parada, M.A., Skewes, M.A., 2007. Chilean volcanoes. In: Moreno, T., Gibbons, W. (Eds.), The Geology of Chile. Geological Society of London, London, pp. 147–178.

Tagiri, M., Moreno, H., López-Escobar, L., Notsu, K., 1993. Two magma types of the high-alumina basalt series of Osorno Volcano, Southern Andes (41°06′ S) plagioclase dilution effect. J. Mineral. Petrol. Econ. Geol. 88 (7), 359–371.

Völker, D., Kutterolf, S., Wehrmann, H., 2011. Comparative mass balance of volcanic edifices at the southern volcanic zone of the Andes between 33°S and 46°S. J. Volcanol. Geotherm. Res. 205, 114–129.

Wiese, H., 1962. Geomagnetische Tiefentellurik Teil II: Die Streichrichtung der untergrundstrukturen des elektrischenWiderstandes, erschlossen aus geomagnetischen Variationen. Pure Appl. Geophys. 52, 83–103.